Blue color of ribbontail stingray skin stems from a core-shell photonic glass ultrastructure

Venkata A Surapaneni (amar.sv@cityu.edu.hk)
1. Department of Infectious Diseases and Public Health, City University of Hong Kong 2. Department of Biomaterials, Max Planck Institute of Colloids and Interfaces https://orcid.org/0000-0002-6241-9048

Michael J Blumer
Institute of Clinical and Functional Anatomy, Medical University Innsbruck

Kian Tadayon
B CUBE - Center for Molecular Bioengineering, Technische Universität Dresden

Ashlie McIvor
MARE - Marine and Environmental Sciences Centre

Stefan Redl
Institute of Neuroanatomy, Medical University Innsbruck

Hanne-Rose Honis
Institute of Clinical and Functional Anatomy, Medical University Innsbruck

Frederik H. Mollen
Elasmobranch Research Belgium

Shahrouz Amini
Department of Biomaterials, Max Planck Institute of Colloids and Interfaces

Mason N Dean (mason.dean@mpikg.mpg.de)
1. Department of Infectious Diseases and Public Health, City University of Hong Kong 2. Department of Biomaterials, Max Planck Institute of Colloids and Interfaces

---

Research Article

Keywords: elasmobranch, blue, structural color, photonic glass, ecology, evolution, guanine, bioinspiration

Posted Date: May 24th, 2023

DOI: https://doi.org/10.21203/rs.3.rs-2969747/v2

Blue color of ribbontail stingray skin stems from a core-shell photonic glass ultrastructure

Venkata A. Surapaneni[1]*†, Michael Blumer[2]*, Kian Tadayon[3], Ashlie McIvor[4], Stefan Redl[5], Hanne-Rose Honis[2], Frederik H. Mollen[6], Shahrouz Amini[7], Mason N. Dean[1,7]†

[1]Department of Infectious Diseases and Public Health, City University of Hong Kong, Kowloon, Hong Kong

[2]Institute of Clinical and Functional Anatomy, Medical University Innsbruck, A-6010, Innsbruck, Austria

[3]B CUBE - Center for Molecular Bioengineering, Technische Universität Dresden, Germany

[4]MARE - Marine and Environmental Sciences Centre, 9020-105, Funchal, Portugal

[5]Institute of Neuroanatomy, Medical University Innsbruck, A-6010, Innsbruck, Austria

[6]Elasmobranch Research, 2820 Bonheiden, Belgium

[7]Department of Biomaterials, Max Planck Institute of Colloids and Interfaces,14476, Potsdam, Germany

*Equal contribution

†Corresponding authors: Venkata A. Surapaneni, amar.sv@cityu.edu.hk; Mason Dean, mason.dean@mpikg.mpg.de, mndean@cityu.edu.hk

ABSTRACT

Blue structural colors, produced by diverse tissue nanostructures, are known from all major vertebrate clades except cartilaginous fishes (e.g. sharks, rays). We describe a bright angle-independent structural blue from ribbontail stingray skin, arising from a novel cell type with unique quasi-ordered arrays of nano-vesicles enclosing guanine nanoplatelets. This natural architecture —an intracellular photonic glass— coherently scatters blue, while broadband absorption from closely-associated melanophores obviates the low color-saturation typical for photonic glasses. This first demonstration of structural color in elasmobranchs (the oldest extant clade of jawed vertebrates) illustrates that the capacity for guanine-based colors likely arose extremely early in vertebrate evolution. The structure-function mechanisms underlying ribbontail stingray coloration point to selective pressures driving elasmobranch visual ecology and communication, but also strategies for biomimetic color production.

INTRODUCTION

The colors of living organisms are diverse and can play crucial roles in communication, predator evasion, and thermoregulation (*1*). The various mechanisms nature uses to produce color, therefore, can offer fundamental insights into the biological tools that shape diverse ecological interactions, as well as the physical and phylogenetic relationships that govern them. Color in nature can be either due to selective 'absorption' of light by pigments (pigmentary color), selective 'scattering' of light from nanoscale structures (structural color), or a combination of these mechanisms. In particular, blue colors are of special interest in being widespread, visually perceived by many taxa, and involved in a variety of functions. Pigmentary blues are however relatively uncommon, meaning most natural blues have a structural origin (*2, 3*). Yet, the exact nanostructural features and materials responsible for producing natural blues vary considerably across taxa, indicating that nature has arrived on multiple solutions for creating similar striking colorations. Many bony fishes, for example, especially shallow water and reef-associated species have diverse blue color patterns (*4-6*), derived from pigmentary and purine-containing cells of bony fishes (*7-10*). In contrast, the mechanisms responsible for the blue skin colorations that have been anecdotally described in multiple disparate species of sharks and rays (elasmobranch fishes; *11,12*) have yet to be examined. Given that modern elasmobranch fishes and bony fishes diverged from a common ancestor hundreds of millions of years ago, and given the major intrinsic differences in elasmobranch skin, scale and skeletal structure relative to those of bony fishes, we hypothesized that the blues of sharks and rays very likely represent novel structural color mechanisms for fishes (although, alternatively, a mechanistic convergence with bony fish colorations would be equally exciting).

In this study, we explored the ultrastructure and basis of color production of the skin of the blue-spotted ribbontail ray, *Taeniura lymma* (Fabricius, ex Forsskål, *13*) (Fig. 1a-d), a small-sized benthic ray common to coral reef habitats across the Indo-West Pacific from South Africa to Papua New Guinea (*12, 14*). Juvenile rays typically occupy shallow reef-adjacent and intertidal habitats (i.e., mangrove, seagrass, and rocky shorelines; *15-17*), whereas adults are often found in deeper reef environments (< 50m) and utilize shallow sandflats for foraging, mating, and pupping (*14,18*) (Fig. 1e). Unlike the relatively uniform and muted body colors of many oceanic stingrays, the ribbontail ray has a conspicuous color pattern, with bright electric blue coloration, accenting its dorsal body skin color (*12)*; our field studies show substantial color variation in both the blue and non-blue regions, with the latter ranging from greenish-, yellowish-brown or even orange dorsal body skin (Fig. 1a-d). In providing the first mechanistic description of color in elasmobranchs, we demonstrate structural color for the first time in this group, while also providing a first characterization of what we believe to be a novel cell type responsible for color production.

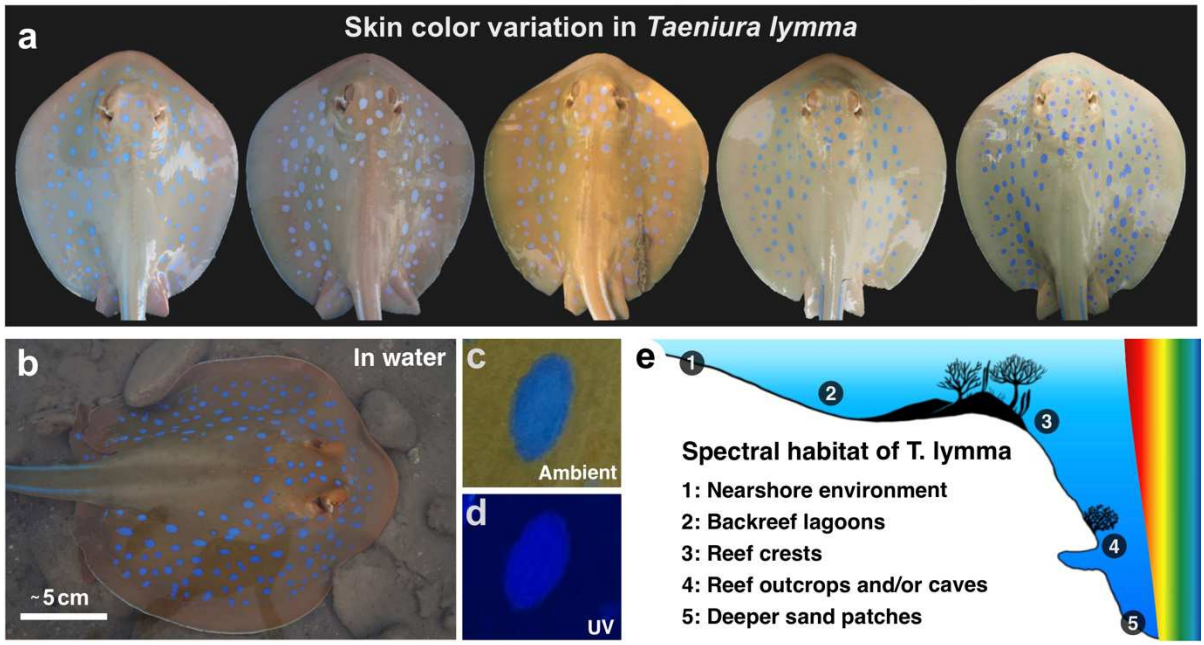

Fig 1 Skin color and habitat of ribbontail stingray *Taeniura lymma*: The natural variation we observe in the skin color of ribbontail stingrays **(a)** —in the blue spots as well as in non-blue regions— suggests (structural or pigmentary) variability in the color producing tissue. In a typical color variant **(b)** in ambient light, the spots and other skin regions appear bright electric blue and green-brown respectively **(c)**. Under a UV light source, however, the spots are saturated with a strong electric blue hue and other skin regions appear dark blue **(d)**. Ribbontail stingrays occupy a variety of spectral habitats **(e)** - the blue wavelengths available in all of these regions suggest that the blue spots on their skin are ecologically relevant.

RESULTS AND DISCUSSION

Visual and optical properties of the blue spots of *Taeniura lymma*

Natural color is a product of context: of incident light wavelengths, the properties of the color-producing tissue (which dictate the range of wavelengths reflected), and the position and sensory capabilities of the observer, whether predator, prey or potential mate. Given the use of multiple reef microhabitats by the ribbontail ray, one can assume variations in the spectral habitat that the species may occupy (*19*) (Fig. 1e). For instance, in-water light transmission and attenuation typically increase from backreef to forereef waters, with blue and green wavelengths dominating in eutrophic coastal waters and lagoons, and a greater availability of blue wavelengths when moving to the forereef and offshore waters (*19, 20*). These differences in light availability can also be affected by natural variations in suspended particulates and dissolved organic matter and may lead to variations in the color perception of the ribbontail ray across local and regional scales (*20, 21*). Understanding how natural color varies with context can therefore provide

critical baseline information, not only on the properties and basis of color production, but also on the role that skin color plays in an animal's ecology and its structural and/or compositional stability.

In this study, all sampled specimens, including both juvenile and adult stingrays, exhibited the bright electric blue coloration distinctive for this species, displaying spots on their dorsal body, lateral stripes on their tails, and an ovular swath of color surrounding the lower caudal finfold to the tip of the tail and the stinging spine (Fig. 1b). Color profile measurements on ribbontail ray skin in water showed that, in sunlight (Fig. 2a), the juvenile animal's blue spots showed peaks in the blue region (~487 nm), while the non-blue portions of skin strongly reflected in the red (~674 nm) (Fig. 2c). In lab conditions (i.e., under a controlled range of incident wavelengths, Fig. 2b), the blue spots predominantly reflected short wavelengths in the blue-cyan region of the visible spectrum (juvenile: ~452 nm; adult: 447 nm), whereas the non-blue regions reflected longer wavelengths. Surprisingly, a strong UV peak (juvenile: ~344 nm and adult: ~335 nm) was common to both blue and non-blue regions of the skin (Fig. 2d,e). This variation between sunlight and lab measurements is likely due to the nature of the incident light in the two conditions, being directional and broad-spectrum in the lab, but diffuse with more variable wavelengths in ambient conditions. Measurements at various angles of light incidence indicated that the blue spots are non-iridescent, confirming our visual observations from intact specimens that the color is unchanging with viewing angle (Fig. 2f). Although non-iridescence is often taken to indicate a lack of structural color, it can also be due to an irregularity of the structure (*22*) that results in scattering of light, regardless of the angle of incidence; we explore these options at a tissue level below.

The ecology and visual capabilities of this species provide some suggestions as to the roles its electric blue coloration may play for this species. Ribbontail ray can perceive blue wavelengths with absorbance maxima at wavelengths ~479 nm (S-cone photoreceptor cells), 500 nm (rod cells) and 557 nm (L-cone cells) (*23*). Moreover, the ribbontail ray has a specialized visual apparatus for low-light scotopic vision and a greater spatial resolving power compared to other benthic batoids (*23, 24*), which may facilitate improved transmission of visual cues between conspecifics, especially during crepuscular periods where rays are often seen gathered in shallow waters (*17*). In these regions, short-wavelength photons dominate the underwater spectrum (*25*) and the resulting blue illumination may emphasize and further saturate the blue spot pattern. The mixture of yellow/green and blue coloration in the ribbon tail ray is also an effective color combination that transmits well in reef waters, providing the most chromatic contrast for a range of animal visual systems (*26*) and possibly serving as an aposematic warning system to nearby predators. However, given the reduced color-vision range of other reef fish, the once conspicuous yellow/green and blue colors of the ribbontail ray would quickly merge and fade into the background over the span of a few meters towards the

achromatic point (*27*), suggesting that the blue spot coloration of the ribbontail ray acts primarily as a near-field signal for inter- or intra-specific communication.

Our observations also demonstrate a uniform reflectance of soft UV (UV-A), suggesting that the components responsible for UV reflection should be identical in both blue and non-blue regions of the skin. This was unexpected and suggests the two dominant reflectance peaks (blue and UV) serve different functions. Ribbontail ray visual pigments block UV radiation (*28*) and therefore UV-reflections from their skin would not be perceived by conspecifics, or even by potential predators (e.g. sharks), since many of those lack UV perception (*28, 29*). Instead, since behavioral observations show that the ribbontail ray rarely covers itself in the sand like other stingray species (*14*), UV-A is not especially damaging to skin and coastal sand is known to reflect UV light (Baltic seaside at Juodkrantė, *30*), we hypothesize that the UV-reflectivity of ribbontail ray skin provides camouflage in sandy, intertidal habitats, perhaps a useful deterrent against predation by birds (which can perceive UV; *31*).

On close examination of skin regions with a stereomicroscope, the blue color, especially in the larger body spots, had the quality of a milky paste, dabbed onto the skin surface, with black dendritic splotches coalescing in a dense layer beneath it; this suggested that the regions responsible for the blue color may be quite superficial (Fig. 2g,h). The microscale splotches also extended into non-blue regions, albeit only sparsely (Fig. 2h). As our specimen lacked skin denticles, the soft nature of its skin allowed us to gently peel away the outer skin layers (~0.4 mm, with a black spot left behind on the specimen after peeling) and transfer them onto synthetic substrates to explore the effect of the black dendritic layer on the overall color appearance. The isolated tissue, when affixed to black carbon tape, exhibited a similar blue to that of the intact animal, whereas on a white substrate, the color was much paler and the tissue was almost transparent (Fig. 2i). Previous studies on biological and artificial optical materials have shown that black backgrounds can serve to absorb longer and incoherently scattered wavelengths and help in the saturation of blue color (*32, 33*). In our study, while the paler color of ribbontail ray tissue on white backgrounds suggests a superimposition of all colors in the spectrum, the brighter blue color on carbon tape indicates that the tissue's natural black backing acts as a broadband absorber of longer wavelengths and is therefore an important component of the blue coloration.

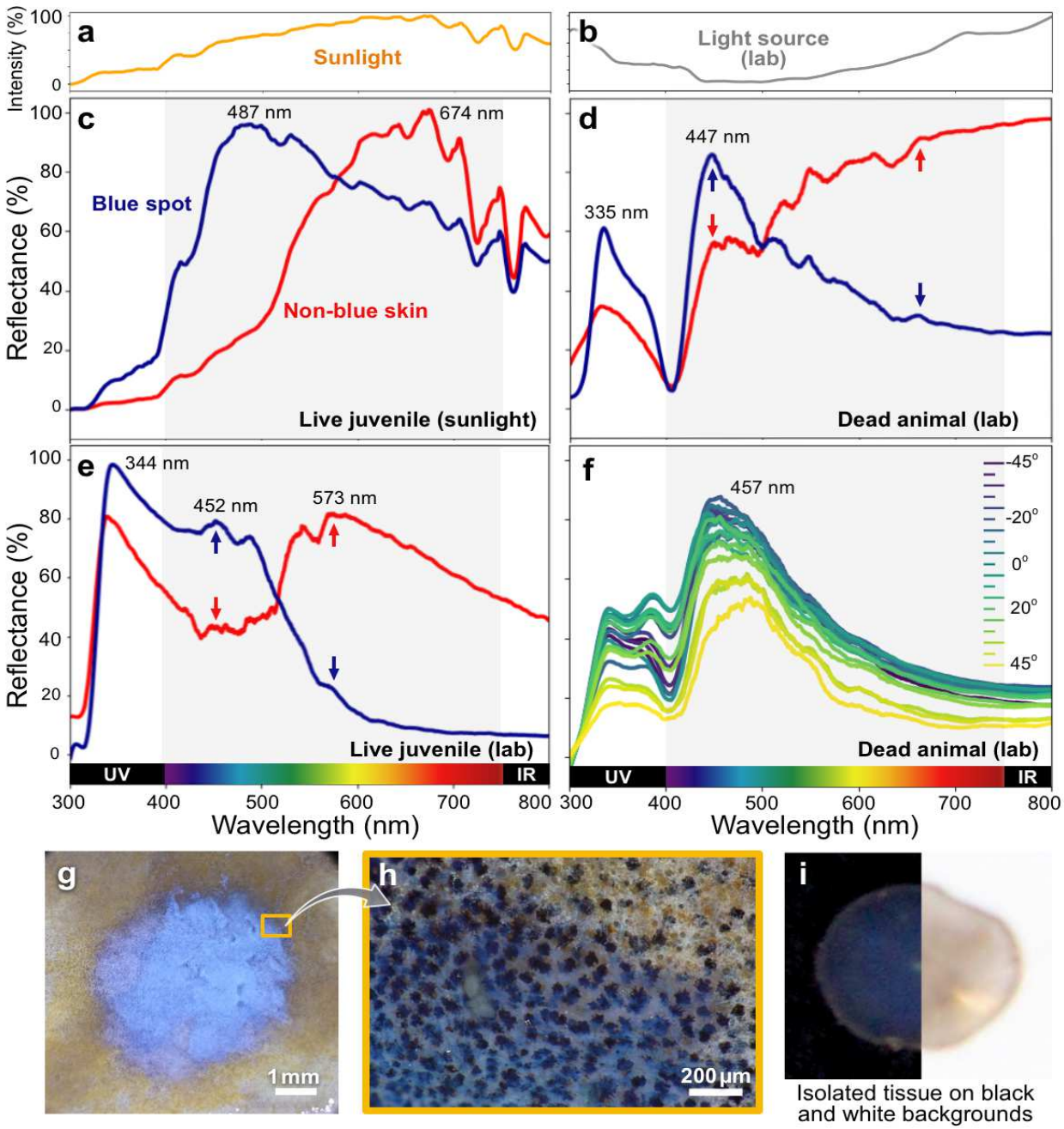

Fig 2 Color properties of ribbontail ray skin in water: The blue and non-blue regions of ribbontail ray skin showed strong variation in the wavelengths reflected, whether in sunlight **(a)** or lab **(b)** conditions. The normalized reflectance plots **(c-f)** showed that in sunlight, the spots on the skin of a live juvenile reflect strongly in the blue-cyan region, while the non-blue regions reflect yellow-red wavelengths of the visible spectrum **(c)**. Lab measurements **(d-f)** showed strong reflection of short wavelengths (blue) and strong absorption of long wavelengths from the spots (blue arrows), but vice versa from the non-blue skin regions (red arrows). All skin regions, however, strongly reflected UV wavelengths **(d,e)**. Reflectance measurements at various angles of incidence on the skin of the adult specimen **(f)** demonstrated the non-iridescent color of spots. The blue spot color had a milky paste-like quality upon closer inspection **(g)** and at higher

magnifications, could be seen to involve a superficial blue layer underlain by numerous black splotches that extended only sparsely into the non-blue region (upper right corner of **h**). Excised superficial skin tissue placed on black carbon tape versus a white background **(i)** showed that a black background is necessary for the blue color of the skin.

In contrast to our fresh specimens, in one specimen that was frozen immediately after death for ~4 years, all characteristic blue regions were dark blue or nearly black in color (Fig. S1). Strikingly, however, spots cut from this hugely shriveled specimen returned to their natural electric blue immediately when placed in water; moreover, this color switching was reversible, with the blue being recoverable even after multiple freeze-thaw cycles. Likewise, in the tissue affixed to black carbon tape, the color reversal process was repeatedly achieved following de-/rehydration cycles, with the drying of the tissue producing black and re-wetting recovering blue hues, respectively. In fact, even after being left dry at room temperature for six months, the color of the excised tissue returned to blue soon after rehydration. Tissue colors that vary with hydration can be the result of changes in structure and/or refractive index when water leaves the tissue (*34, 35*), or pigmentary changes arising from pH differences (*36*). Our observations that the blue skin color of ribbontail ray is highly robust and reversible with de- and re-hydration are not enough to prove a structural origin of color —thus, tissue-level characterizations were necessary.

Unique ultrastructure of blue spots of ribbontail ray skin

The skin of all vertebrates contains specialized color-producing cells called chromatophores. Chromatophores exist in various forms: light-absorbing pigment-containing melanophores (black or brown pigments), erythrophores (red or yellow pigments), cyanophores (blue pigments), and colorless reflective purine-containing leucophores and iridophores (*7, 8, 9*). The distribution of these cells in skin layers (epidermis and dermis) and their interactions with other tissue components are responsible for the diverse and colorful patterns of fish skin (*2, 37, 38*).

Despite the deep interest in the denticle morphology and hydrodynamics of shark skin (*39, 40*), the histology of shark and ray skin is surprisingly poorly described. Our light and transmission electron microscopy investigations showed that, as in other fishes, the skin of ribbontail ray (Fig. 3a) consists of an epidermis (E: 100 - 250 μm thick), separated from a thicker underlying dermis (D: 350 - 500 μm) by a thin basement membrane (B: 0.3 μm). In both blue and non-blue skin regions, the dermis was visibly stratified. A horizontal layer (H) with a unique ultrastructure (see below) in the upper dermis was effectively sandwiched between two densely collagenous layers: a thin upper layer of collagen fibers (UC, 1 - 5 μm) below the basement membrane and a thick (LC, 100 - 150 μm) layer of interwoven collagen fiber bundles in the lower dermis.

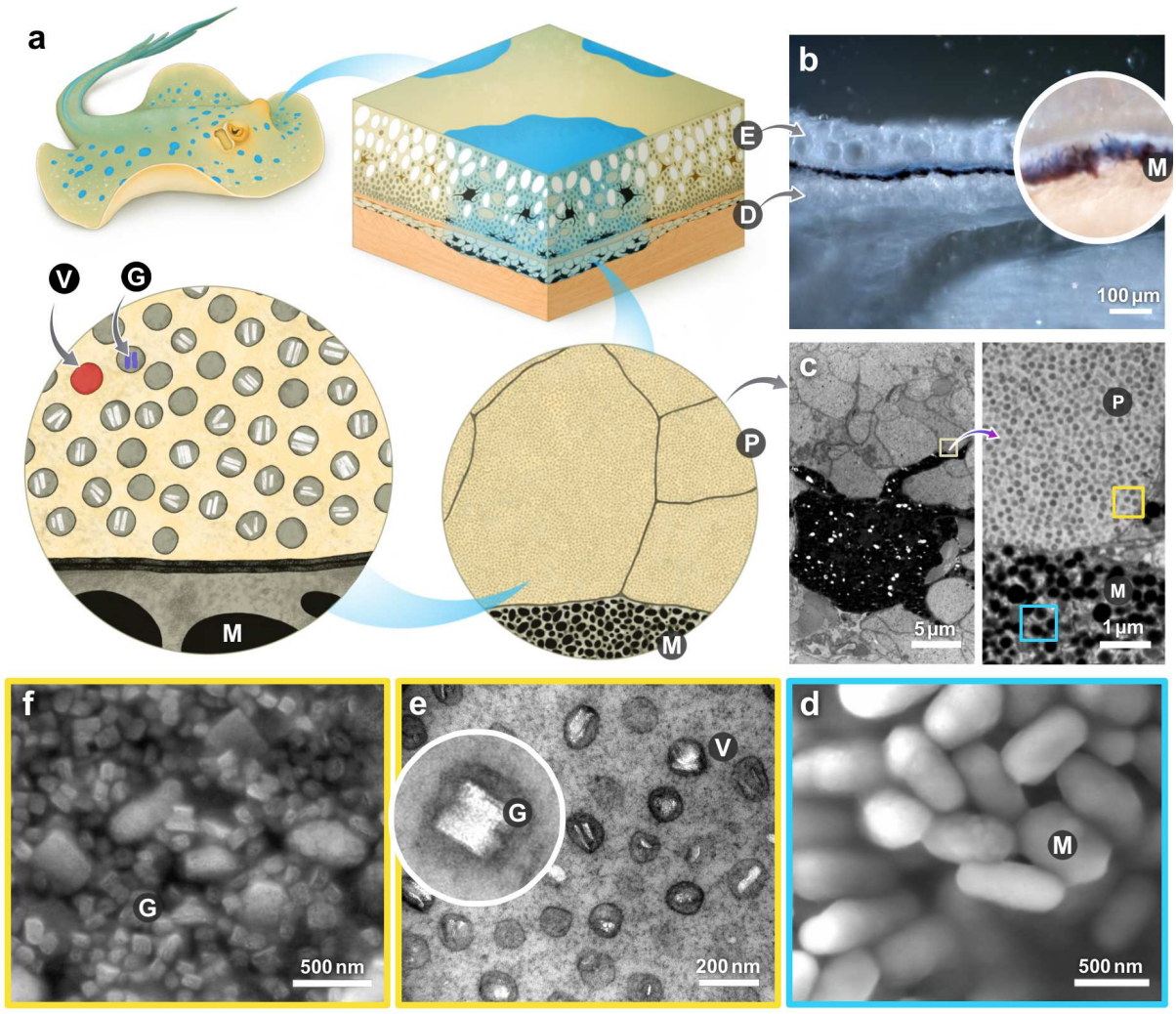

Fig 3 A schematic of a blue spotted ribbontail ray skin: (a) shows multiple levels of hierarchical architecture responsible for blue color production. Epi-illuminated blue spots **(b)** showed a blue hue just above the dark melanin region (M) sandwiched between the epidermis (E) and dermis (D) suggesting that the source of blue color is tightly associated with the melanin layer. TEM **(c,e)** and SEM **(d,f)** characterization showed that in the blue spots, below the upper collagen layer (UC), pale cells (P) are encased around black melanophores (M) with numerous spherical and ellipsoidal-shaped melanosomes **(c,d)**. The pale cells contain numerous nanovesicles (V) surrounded by cytoplasm and the nanovesicles are filled with guanine nanoplatelets (G) mostly occurring in pairs **(c-f)**. The inset in **(e)** shows a fused pair of platelets in a single vesicle. The image **(f)** shows guanine platelets with vesicle and pale cell membranes disrupted in an isolated tissue on a carbon tape.

We found three distinct cell types in the skin layers: mucous cells, melanophores (with either black or brown pigments), and specialized cells we refer to here as ‘pale cells’. These three cell types varied in their arrangement, preponderance, and density in the epidermis and dermis and, more importantly, in ways that distinguished blue from non-

blue regions. The epidermis of both blue and non-blue areas were histologically relatively similar, dominated by large mucous cells superficially, but containing a scattered mix of mucous cells, melanophores, and pale cells closer to the basement membrane. We verified that the dark dendritic splotches observed by stereomicroscope (see above) were melanophores, exhibiting stellate morphologies and squeezed between the other cell types. The pale cells were so named because of their nearly featureless appearance in histology/light microscopy, such that they initially looked to be vacuolated (our electron microscopy observations revealed this not to be the case; see below). Although blue and non-blue regions were compositionally similar, the blue epidermis tended to contain fewer mucus-producing cells in some regions/specimens, more pale cells, and "black melanophores" (*sensu 41, 42*) that were more dendritic and darker (in contrast to the non-blue region, which contained less-electron-dense "brown melanophores" and more sparsely distributed "black melanophores").

Unlike the epidermis, the upper dermis exhibited key ultrastructural differences between blue and non-blue regions of the skin. In blue regions only, the upper dermis (~35 μm thick) was densely packed with pale cells, amalgamated into large multi-cell complexes which often enclosed branched black melanophores. The tight association of pale cells with melanophores and their extended dendritic processes resulted in intracellular melanosomes being distributed throughout the pale cell layer, with the local concentration of melanosomes higher deeper in the tissue (corresponding to the "black dendritic backing layer" we observed in the previous section). In contrast, in non-blue regions, the horizontal layer (H) was only one-third as thick (up to 15 μm wide), contained more sparsely distributed black and brown melanophores, and a continuous layer of pale cells. The collagen layers (UC and LC) that surround the horizontal layer (H) were present in both blue and non-blue regions of the skin with no obvious differences, although the lower collagen layer was slightly thicker in the non-blue region. Our electron microscopy investigations revealed that pale cells do in fact contain a highly organized internal structure, which only became visible when samples were carefully and immediately fixed and then contrast-stained. In such samples, the lumen of pale cells was observed to be entirely full of nano-vesicles (~126.79 ± 13.08 nm in diameter), the morphology and arrangement of which varied with location in the tissue: whereas pale cells in the non-blue region contained vesicles that were more elongate and random in their arrangement, those in blue skin regions were spherical and mono-disperse with a strikingly uniform arrangement and packing density (~28 vesicles/μm). In the upper dermis of the blue skin regions, intracellular melanosomes (*M* in Fig. 3c,d) were jet black and of variable cross-section, ranging from ellipsoidal to spherical shape and roughly similar in size (500-600 nm), several times larger than pale cell vesicles. In well-fixed specimens, the extremely tight encasement of pale cells around melanophores was particularly impressive — with the many surrounding pale cells creating a nearly uniform, nano-vesicular corona around each pigment cell. In contrast to the non-blue regions,

epi-illuminated light microscopy observations of skin cross-sections showed a conspicuous blue hue in blue spot regions, just above the dense black melanophore layer, suggesting that the blue color originates in the overlying pale cell layer (Fig. 3b).

TEM observations supported by SEM imaging of the isolated skin revealed that the spherical nano-vesicles contained crystalline structures (85.01 ± 14.58 nm wide, Fig. 3e,f), often rhomboidal in cross-section, occurring mostly in pairs within the matrix of each vesicle and with no defined orientation. However, in many vesicles, the crystals are extracted during sample preparation, leaving an empty space inside vesicles in TEM images. EDX and Raman spectroscopic measurements (Fig. S2) confirmed that these nano-crystals were nitrogen-rich and made of anhydrous beta-guanine (*43, 44*). Beta-guanine is a common structural-color-producing purine in bony fishes, typically manifesting as long guanine platelets (each tens of μm long and tens of nm thick), conspicuously stacked inside of iridophore cells. During development, the guanine platelets nucleate from an amorphous precursor inside small vesicles in iridophores, grow, and then coalesce to form single crystal platelets. Crystal growth propagates, partitioned by intravesicular bands, resulting in a layered arrangement of long guanine crystals (*45-49*). These large crystalline stacks act as multilayer reflectors to produce color and/or a silvery appearance in the skin (*50, 51*).

Pale cells are clearly a widespread and characteristic cell type in ribbontail ray skin and, we propose, at least partly responsible for this species' blue coloration. With the exception of black and brown melanophores, we have not observed any pigmentary cells that might contribute to the blue color in ribbontail ray nor found any previous description of pale cells in elasmobranch or bony fishes in the literature; the careful preparations required to visualize pale cell contents, however, could mean these cells are more prevalent than realized, at least in elasmobranchs. Although the distribution and composition of pale cells indicates they are likely involved in a guanine-based blue structural color, the morphology and arrangement of guanine crystals in the cells of ribbontail ray is strikingly different from that of bony fishes. To the best of our knowledge, such a uniform and stable colloidal arrangement of guanine nano-crystals embedded in nano-vesicles has never been reported in fishes. Oddly, the most similar example we find in the literature is from an invertebrate, the Spanish shawl nudibranch mollusk (*Flabellina iodinea*), where short stacks of guanine nanocrystals, bound by membranes, form 'punctate reflectors' (*52*). Although these nanoreflectors are also localized in specialized cells near the epithelial basal membrane, as in ribbontail ray, their vesicles are less organized in their arrangement, instead packed in high densities within their specialized cells, but also scattered and mobile throughout the epithelium. The distinct morphology of ribbontail ray pale cells argues that their mechanism of guanine-based color production likely differs from that of other fishes, as well as the nudibranch example with which they are most similar; we examine possible mechanisms more deeply in the next section.

In addition to our dehydration-rehydration experiments above, the response of our specimens to fixation support our assertion that pale cells are involved in producing a structural blue in ribbontail ray. In our study, blue spots from adult specimens fixed and stored for ~4 years in a buffer solution lost their blue color with time. Such color loss is common in fixed specimens with structural color, attributed to architectural or refractive index changes that occur as a result of fixation (*53-56*). In our ribbontail ray samples, ultrastructural characterisation showed that pale cell nano-vesicles in blue regions were less densely arranged than in more freshly-fixed specimens and intravesicular guanine crystals were rare. In contrast, tissue from samples frozen for the same amount of time remained blue (albeit comparatively dark), with SEM of isolated skin verifying the presence of guanine crystals. Furthermore, the freshly-fixed spots from the juvenile specimen remained electric blue for several weeks after fixation with glutaraldehyde and therefore we suppose their ultrastructures are close to natural tissue architectures. The exact cause of color loss in long-fixed tissue remains to be identified, but these observations argue that the spacing of nano-vesicles and/or the presence of guanine nano-crystals (or the composite of crystals and vesicles, see below) are vital for color-production in ribbontail ray, a hypothesis we test below.

Coherent scattering from core-shell photonic glass ultrastructure of blue spots

In natural structural colors, the color produced (i.e., wavelengths scattered by the nanostructures) and the color saturation (i.e., the intensity of color) depend on the morphology and arrangement of the scatterers and their refractive index relative to their surrounding medium (*57, 58*). When nanostructures have a long-range order, as in a photonic crystal, the light waves interfere coherently to produce angle-dependent color or iridescence. In contrast, when nanostructural arrangements are completely random, incident light waves scatter incoherently (e.g., Rayleigh or Tyndall scattering) and the reflected color is non-iridescent. Accordingly, it was long believed that non-iridescent natural colors are caused only by incoherent scattering from zero-order architectures (colloidal nano-spheres in damselfly integuments: *59*; spongy keratin-air matrix of feather barbs: *45, 60*). This hypothesis was recently disproved by Prum et al. (*61-63*), who performed 2D Fast Fourier Transform analyses on transmission electron micrographs of structural colored tissues to calculate dominant frequency components in the arrangement of nanostructural arrays, revealing aspects of order and disorder otherwise imperceptible in direct observations of electron microscope images. Since electron density (gray-scale) variation in properly-stained electron micrographs is indicative of differences in refractive index (RI), the patterns observed in resultant 2D FFT power spectra can be used to distinguish between completely ordered, quasi-ordered and disordered structures, with peak widths corresponding to the spatial frequency of refractive index differences. In this way, Prum et al. (*54, 56, 61*) were able to confirm that the keratin-air structures in feather barbs and nano-spheres in damselfly integuments

exhibit a quasi- or short-range order in spatial scales comparable to visible wavelengths to produce a coherently-scattered, but viewing angle-independent color.

We apply a similar approach to Prum et al. (*54*) in our examination of ribbontail ray micrographs, using 2D FFT analysis to explore the degree of order and predicted optical appearance of tissues we observed in our anatomical characterizations. Nano-vesicle arrays in pale cells showed a ring-like power spectrum (Fig. 4a), confirming they are mono-disperse, quasi-ordered and with a spatial periodicity that the Fourier power spectra prediction produces a mean reflectance peak at a wavelength of 468 nm, closely corresponding to an electric blue color (Fig. 4b). This supports our hypothesis that the spatial correlation between vesicles leads to constructive interference of blue light reflected from the nanostructural arrays in pale cells. Furthermore, the consistent FFT pattern observed from various TEM images —involving a nearly-circular single Fourier ring— indicates that the spatial arrangement of vesicles in pale cells is isotropic, resembling a 'direct' photonic glass ultrastructure (*64-66*). This explains the origin of the distinct and angle-independent color of blue spots in ribbontail ray. A direct photonic glass consists of mono-disperse colloidal structures in an isotropic disordered arrangement, but with a short-range order and higher refractive index compared to the surrounding matrix. It is this material constellation that produces the interesting combination of color characteristics in ribbontail ray, where the structural correlations from the quasi-order of vesicles with guanine crystals in the pale cell lead to coherent scattering of light, but the isotropic nature of the nanostructures results in angle-independence of the structural color (*67*). As a counterpoint, in a poorly-preserved adult specimen where tissues had lost their blue hue, guanine crystals were lacking, and vesicles were less densely packed, the Fourier spectra from pale cell micrographs were disk-like (Fig. S3), further illustrating that the quasi-order of guanine-containing vesicles is essential for the blue color production.

Recently, it was suggested that guanine crystals in the scales of Koi fish *Cyprinus rubrofuscus* and the skin of white widow spiders *Latrodectus pallidus* crystallize from an amorphous precursor distributed within vesicles (*47, 48*). If guanine crystal maturation also takes place in the same way in ribbontail ray pale cells, we suppose that the refractive index of intravesicular space and guanine depends upon the stage of crystal development. The presence of guanine crystals inside vesicles thus results in a non-monotonous variation in refractive index, with most intravesicular space (i.e., the region between guanine and outer vesicular membrane) having an intermediate refractive index when compared with their guanine 'cores' and the surrounding cytoplasm, and the guanine cores may act as the dominant scattering sites. As such, in matured vesicles, the guanine nanocrystals' morphology, high refractive index, and lack of defined orientation may help to significantly enhance scattering in all directions, while the quasi-order of the vesicles provides the resonance that is necessary for angle-independent blue structural color (Fig. 4c). Also, the fact that vesicles do not appear to coalesce

suggests that an unknown mechanism maintains the stability of the colloidal system, perhaps the structure and material properties of the cytoplasm and/or electrostatic repulsion between the vesicles. The mechanism determining crystal shape/growth is still unclear, but our observations of a consistent vesicle morphology in juvenile and adult individuals indicate that the stability of the vesicular core-shell ultrastructure is preserved throughout the ontogeny of the animal. Thus, it appears that the vesicles act as stable containers for the scattering guanine cores, while the dense cytoplasm controls the inter-vesicular spacing, critical for controlling the wavelengths scattered (*67-69*).

It is conceivable that the thick collagen fiber bundles in the lower dermis of the skin also contribute to the blue color of ribbontail ray. In some bird and mammalian skins, a thick layer of quasi-ordered collagen fibers scatter light coherently to produce structural blue colors (*55, 70*). Similarly, in electric rays (*Torpedo ocellata*, a batoid relative of ribbontail ray), it was suggested that collagen fibers are responsible for the bright blue spots on the skin (*2*). In the ribbontail ray, 2D FFT spectra showed that the arrangement of collagen fibers in the lower dermis is also quasi-ordered, however, the mean predicted reflectance from the Fourier power spectra showed peaks in the UV region (~344 nm) and in the violet region (~400 nm) of the visible spectrum (Fig. 4d,e). Moreover, the architecture of lower dermis collagen fiber bundles is almost identical in both blue and non-blue regions of the skin, only slightly thicker in the non-blue region, indicating that the blue color cannot originate from the collagen layers. In addition, the pervasiveness of melanosomes — in a dense layer of black melanosomes at the bottom of the upper dermis in blue skin regions, and brown melanosomes in the upper dermis in the non-blue regions should restrict most incident wavelengths (including blues) from even reaching the collagen bundles in the lower dermis, with the melanosomes also probably absorbing any light that would be back-scattered from the collagen bundles (Fig. 4c). Rather, our FFT predictions and skin reflectance measurements, argue that the extensive lower dermis collagen layer is responsible for the distinct UV reflectance we measured from all skin regions, and which proved extremely robust to different specimen storage and processing conditions (e.g. present even in spots that had been dried or had their top layer removed).

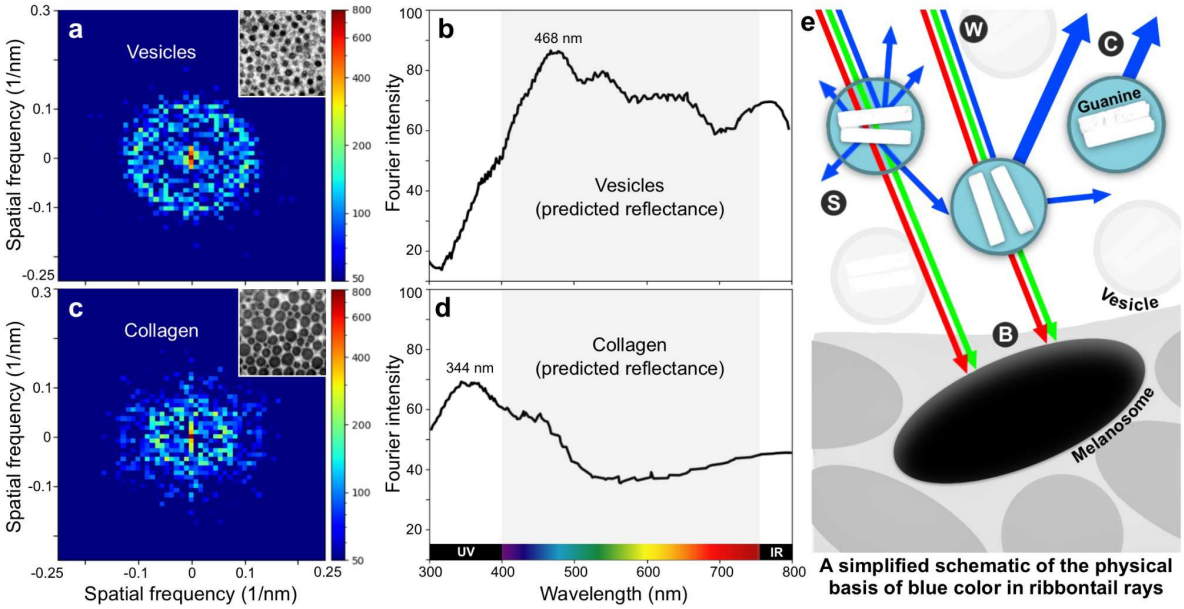

Fig. 4 Coherent scattering of short wavelengths from the blue spots: 2D-FFT analysis of TEM images of vesicles shows a single ring-like spectrum **(a)** demonstrating that the vesicles are arranged in a quasi-order. The predicted reflectance spectrum **(b)** shows peaks in the blue wavelength region closely corresponding to wavelengths reflected by the real skin (see Fig. 2). The lower collagen layer also showed a single ring-like 2D-FFT spectrum **(c)**, however, the predicted peaks **(d)** occurred in the UV region. The schematic (e) shows the possible physical mechanisms of blue color production by ribbontail ray skin: as white light (W) passes through the pale cells, the high refractive index guanine nanoplatelets in vesicles scatter (S) short wavelengths strongly in all directions, while long wavelengths are weakly scattered. Furthermore, the quasi-order of the vesicles **(a,b)** leads to a strong coherent scattering (C) of blue wavelengths, aided by broadband absorption (B) of longer and multiply-scattered wavelengths by melanosomes.

Although photonic glass ultrastructures (e.g. the quasi-order of pale cell vesicles) result in strong scattering, their comparative disorder also translates to a poor spectral selectivity or less-saturated structural color (*71*). In ribbontail ray, this was evidenced by the pale blue of spots when viewed on a white background. Our tissue isolation experiments and characterizations indicate that spectral selectivity is improved by adding a black material in close association, namely the ubiquitous black melanophores within the pale cell layer in the upper dermis of blue tissue regions (Fig. 4c). While the melanophores with their horizontal processes deeper in the tissue absorb wavelengths transmitted through the pale cells and scattered from the lower collagen layer, the intracellular melanosomes distributed throughout the pale cell layer should absorb incoherently- or multiply-scattered long wavelengths, enhancing the saturation of the blue color (*33, 71, 72*). We expect that the high aspect ratio of ellipsoidal melanosomes in black melanophores also helps to further enhance broadband absorption (*73*).

Therefore, we argue that a combination of structural scattering from vesicles with randomly oriented guanine cores and broadband absorption from melanin pigments is crucial for the strong non-iridescent electric blue color of ribbontail ray skin. This unique nano-structural skin architecture represents an interestingly disordered arrangement for color production, with the mechanism not only demanding the evolution of the unusual pale cell type but also its intimate association with melanophores. Our demonstration that certain tissue components and structural arrangements are necessary to produce the ribbontail ray's blue color also argues that subtle structural modifications to the observed tissue nano-architectures may be the root of the natural color variation we observed in the field (Fig. 1a). The presence of pale cells, even in non-blue areas, suggests that they may have (or have had) some other tissue function, but it was their evolutionary co-optation into a structural partnership with melanophores that gave rise to the novel and ecologically important tissue color. Understanding pale cell origins and their prevalence in other species and tissues will therefore be key for understanding the evolution of structural color in elasmobranch skin, but also for designing biomimetic structural blues.

CONCLUSIONS

This first report on the basis of skin color in elasmobranchs also demonstrates a new mechanism of guanine-based structural color production in animals. Although guanine-based methods for generating blue hues are quite common among natural structural color systems, the light-matter interactions involved are surprisingly diverse. For example, whereas the blue coloration of the mantle tissue of nudibranch molluscs is the result of incoherent Rayleigh scattering from disordered vesicular nanocrystals (*74*), the blues of bony fish skin are due to multilayer interference from stacks of large guanine platelets (*51*). In contrast, we show that the blue spots of ribbontail rays are the result of coherent scattering from a quasi-ordered arrangement of nano-vesicles with guanine nanoplatelets in pale cells, coupled with broadband absorption by melanophores. In relation to other guanine-based natural blues, the robust and angle-independent structural blue color of ribbontail ray underlines that crystal morphology, ordering and tissue associations offer a multivariate palette for producing color through evolution. Given that biogenic guanine crystals can also vary in their purity (often involving surprisingly large amounts of other purines; *75*) and that the mechanisms underlying elasmobranch skin coloration remain largely unexplored, research into the composition of guanine crystals in ribbontail ray and other elasmobranchs, and into the development, function(s) and prevalence of pale cells will bring new perspectives on the early evolution and diversity of color production mechanisms in vertebrates.

Pale cells, the source of blue color in ribbontail rays, boast a unique morphology relative to other structural color-producing cells in fishes, but their use of guanine as a scattering material argues they may in fact be modified iridophores. Our results demonstrate that

the nanoscale of guanine platelets and the spacing of their vesicles are key for strong angle-independent blue color production. Since the blues produced by bony fish iridophores are due to multilayer interference from large, agglomerated guanine crystals, this suggests that pale cells could represent iridophores where the developmental process has been somehow truncated to produce smaller crystallites, perhaps through heterochrony or restrictions on crystal growth and/or vesicle coalescence (see *48, 49*). The ontogeny of pale cells, but also the composition of their vesicular- and intervesicular-matrices, are therefore important targets for future work, as they could offer clues to the matrix-based control of crystal growth and the evolutionary roots of structural color in elasmobranchs (e.g. whether components of the more-common non-blue tissues were co-opted to produce blues), but also core factors in the evolution of iridophores and vertebrate structural color. The indication that strong blue and UV reflections occur in different skin tissue layers in ribbontail rays and may serve distinct ecological functions (conspecific and anti-predator signaling vs. UV-camouflage) also argues that different selective pressures may have driven the evolution of local skin anatomy in elasmobranch fishes.

There is considerable interest in fabrication mechanisms that allow precise control of material architecture to produce brighter colors in photonic glasses (*71*). Magnetic tuning, for example, can be used to control the orientation of anisotropic crystals that function as cores in man-made core-shell colloidal photonic systems (*76*). For these pursuits, the ribbontail ray represents an excellent biomimetic model for color-saturated core-shell photonic glass, since its bright blue coloration illustrates that robust coloration is possible from less controlled architectures.

MATERIALS AND METHODS

Sample collection: Fresh specimens of the bluespotted ribbontail ray *T. lymma* were collected from commercial fisheries operating off Singapore (Pulan Ubin–Changi area), Indonesia (Jakarta), and Kenya (Eastern Indian Ocean) between May 2017 and June 2022, following the protocol by Mollen (*77*); these included two females, one adult of approx. and 26.0 cm DW and 72.5 cm TL (TALY 3), and a juvenile of 14.9 cm DW and 35.7 cm TL (TALY 4, ex ERB 1300) presented in this study.

Tissue preparation for transmission (TEM): Immediately after the death of the fish, skin samples of approximately 5 mm^3 including both the blue spot and adjacent non-blue area, were collected and fixed in Karnovsky's solution (2% PFA, 2.5% GA, buffered in 0.1M PBS) for 2 hrs on a shaker at room temperature, and subsequently stored at 4°C. The samples were shipped to the Medical University of Innsbruck, where they were further processed for TEM and the remaining voucher material has been preserved deep frozen at Max Planck Institute of Colloids and Interfaces (MPICI, Potsdam, Germany). The shipped samples were cut into smaller pieces, each containing the blue spot and the adjacent green-brown background. Samples were rinsed in sodium cacodylate

buffer and post-fixed in 0.5% osmium tetroxide and 1% potassium ferricyanide in distilled water overnight at 4 °C. They were rinsed again, dehydrated in graded ethanol series and embedded in EPON resin (#45359, Sigma-Aldrich, Austria). Vertical ultra-thin sections (90 nm) were cut with an ultradiamond knife (Diatome, Biel, Switzerland), mounted on dioxane formvar-coated slot grids (#PYSL2010S-CU, Science Services, München, Germany), and stained with 1% uranyl acetate and lead citrate (Reynolds, 1963).

Ultra-thin sections were examined with a Philips CM 120 transmission electron microscope at 80 kV (FEI, Eindhoven, The Netherlands) equipped with a MORADA digital camera and iTEM software (Olympus SIS, Münster, Germany).

Particle morphology and EDX - ESEM: Outer skin layers (~0.4 mm) of the ribbontail ray skin were isolated in water and gently affixed upside down onto a black carbon tape. The morphology of the inverted tissue (with melanosome granules and guanine platelets detectable on the surface) was then observed at high resolution using an environmental scanning electron microscope (ESEM, Quattro S, Thermo Fischer Scientific, FEI Deutschland GmbH, Germany) with a secondary electron (SE) detector operated at 5kV with a 5.9-mm working distance and low vacuum (0.75 torr pressure). The elemental composition of the samples was obtained from energy dispersive x-ray spectroscopy measurements (EDX) using an EDS detector at 30000x magnification at 15kV.

Raman spectroscopy: Confocal Raman spectroscopy was performed using a confocal Raman microscope (alpha300R, WITec, Ulm) equipped with a 532 nm laser source and a ×20 objective lens (Zeiss EC Epiplan-Neofluar Dic 20x / 0.5). An integration time of 1s, accumulations 70-200 times, laser power of 12 mW, and a grating of 600 g/mm were used for acquisition. The spectrometer was calibrated using a silicon wafer sample. WITec Project Five 5.2 and OriginPro 2020 were used for filtering, analyzing, and plotting the data.

Color measurements: Optical studies were performed on live juvenile and dead adult ribbontail ray using a customized setup including a light source (DH-2000-BAL, Ocean Insight), a spectrometer (OCEAN-HDX-XR, Ocean Insight), and one Y-type compound optical fiber for transmission of the light source and collection of the reflected spectra from the skin surface. The collected spectra were extracted using OCEANVIEW (Ocean Insight) and then plotted using the matplotlib module in Python.

2D FFT analysis:

Square sections were extracted from multiple individual TEM images of vesicles and were contrast-adjusted using ImageJ software to enhance the distinction between the tissue components. 2D FFT analysis was performed using the scipy module in Python to obtain the FFT spectra of the vesicles. Similarly, the FFT spectra of collagen fibers

were obtained. By using refractive index (RI) values of 1.42, 1.35 and 1.3 for collagen, vesicles and cytoplasm respectively, histograms were generated from the greyscale 2D FFT spectra to obtain the weighted mean refractive index of the tissues. Radial mean data of Fourier intensity and wavelength (= 2 x RI/spatial frequency) was obtained from greyscale 2D FFT spectra, the data were normalized from 0-100 in the visible wavelength range and the predicted reflectance spectra were plotted using the matplotlib module in Python.

ACKNOWLEDGEMENTS

We acknowledge Arie de Jong and Jeffrey de Pauw from the Netherlands and Shu Hui Hiew from Nanyang Technological University, Singapore for their support in securing fresh material of ribbontail ray. We acknowledge Susann Weichold and Cécile Bidan, Max Planck Institute of Colloids and Interfaces, Germany for their support with ESEM and optical measurements. We thank A. Knab and Ch. Seifarth for technical assistance. We thank Joana Carvalho for the ribbontail stingray illustration.

FUNDING

HFSP Program Grant RGP0010-2020 (MD)

General Research Fund GRF Grant HK 11102022 (MD)

AUTHOR CONTRIBUTIONS

Conceptualization: MD, SA

Resources: FM, SA, MB

Investigation: VAS, MB, KT, AM, SR, HRH

Visualization: VAS, MB

Software: VAS

Funding acquisition: MD

Supervision: MD

Writing – original draft: VAS, AM

Writing – review & editing: VAS, MB, KT, AM, SR, HRH, FM, SA, MD

COMPETING INTERESTS

The authors declare no competing interests.

REFERENCES

1. T. Caro, The Adaptive Significance of Coloration in Mammals. *Bioscience*. **55**, 125–136 (2005). doi:10.1641/0006-3568(2005)055[0125:TASOCI]2.0.CO;2
2. J. T. Bagnara, P. J. Fernandez, R. Fujii, On the blue coloration of vertebrates. *Pigment Cell Res.* **20**, 14–26 (2007). doi:10.1111/j.1600-0749.2006.00360.x
3. K. D. L. Umbers, On the perception, production and function of blue colouration in animals. *J. Zool.* **289**, 229–242 (2013). doi:10.1111/jzo.12001
4. W. H. Longley, Studies upon the biological significance of animal coloration. I. The colors and color changes of West Indian reef-fishes. *J. Exp. Zool.* **23**, 533–601 (1917). doi:10.1002/jez.1400230305
5. K. Lorenz, The function of color in coral reef fishes. *Proc. R. Inst. G. B.* **39**, 382–296 (1962).
6. N. J. Marshall, Communication and camouflage with the same “bright” colours in reef fishes. *Philos. Trans. R. Soc. Lond. B Biol. Sci.* **355**, 1243–1248 (2000). doi:10.1098/rstb.2000.0676
7. R. Fujii, "Cytophysiology of Fish Chromatophores" in *International Review of Cytology*, K. W. Jeon, M. Friedlander, J. Jarvik, Eds. (Academic Press, 1993), vol. 143, pp. 191–255. doi:10.1016/S0074-7696(08)61876-8
8. R. Fujii, The regulation of motile activity in fish chromatophores. *Pigment Cell Res.* **13**, 300–319 (2000). doi:10.1034/j.1600-0749.2000.130502.x
9. J. T. Bagnara, J. Matsumoto, Comparative anatomy and physiology of pigment cells in nonmammalian tissues. *The pigmentary system: physiology*, 11–59 (2006). doi: 10.1002/9780470987100.ch2.
10. P. Salis, T. Lorin, V. Laudet, B. Frédérich, Magic Traits in Magic Fish: Understanding Color Pattern Evolution Using Reef Fish. *Trends Genet.* **35**, 265–278 (2019). doi:10.1016/j.tig.2019.01.006
11. D. A. Ebert, H.-C. Ho, W. T. White, M. R. De Carvalho, Introduction to the systematics and biodiversity of sharks, rays, and chimaeras (Chondrichthyes) of Taiwan. *Zootaxa*. **3752**, 5–19 (2013). doi:10.11646/zootaxa.3752.1.3
12. P. Last, G. Naylor, B. Séret, W. White, M. Stehmann, M. de Carvalho, *Rays of the World* (Csiro Publishing, 2016).
13. C. Niebuhr, Descriptiones animalium avium, amphibiorum, piscium, insectorum, vermium; quae in itinere orientali observavit Petrus Forskål. Prof. Haun. Post mortem auctoris editit Carsten Niebuhr. Adjuncta est material medica Kahirina atque tabula maris rubric geographica. (Mölleri, Hauniae, 1775). doi:10.5962/bhl.title.63873
14. P. R. Last, W. T. White, G. Naylor, Three new stingrays (Myliobatiformes: Dasyatidae) from the Indo-West Pacific. *Zootaxa*. **4147**, 377–402 (2016). doi: 10.11646/zootaxa.4147.4.2.

15. O. R. O'Shea, M. Thums, M. Meekan, M. van Keulen, Physical and biological effects associated with stingray foraging behaviour at Ningaloo Reef, Western Australia (2012). http://wch2012vancouver.com/index.php.
16. T. F. Dabruzzi, W. A. Bennett, J. L. Rummer, N. A. Fangue, Juvenile Ribbontail Stingray, Taeniura lymma (Forsskål, 1775) (Chondrichthyes, Dasyatidae), demonstrate a unique suite of physiological adaptations to survive hyperthermic nursery conditions. *Hydrobiologia*. **701**, 37–49 (2013). doi:10.1007/s10750-012-1249-z
17. A. J. McIvor, J. L. Y. Spaet, C. T. Williams, M. L. Berumen, Unoccupied aerial video (UAV) surveys as alternatives to BRUV surveys for monitoring elasmobranch species in coastal waters. *ICES J. Mar. Sci.* **79**, 1604–1613 (2022). doi:10.1093/icesjms/fsac098
18. A. Chin, P. M. Kyne, T. I. Walker, R. B. McAULEY, An integrated risk assessment for climate change: analysing the vulnerability of sharks and rays on Australia's Great Barrier Reef. *Glob. Chang. Biol.* **16**, 1936–1953 (2010). doi:10.1111/j.1365-2486.2009.02128.x
19. E. J. Hochberg, S. A. Peltier, S. Maritorena, Trends and variability in spectral diffuse attenuation of coral reef waters. *Coral Reefs*. **39**, 1377–1389 (2020). doi:10.1007/s00338-020-01971-1
20. B. J. Russell, H. M. Dierssen, E. J. Hochberg, Water Column Optical Properties of Pacific Coral Reefs Across Geomorphic Zones and in Comparison to Offshore Waters. *Remote Sensing*. **11**, 1757 (2019). doi:10.3390/rs11151757
21. J. T. O. Kirk, Effects of suspensoids (turbidity) on penetration of solar radiation in aquatic ecosystems. *Hydrobiologia*. **125**, 195–208 (1985). doi:10.1007/bf00045935.
22. S. Kinoshita, S. Yoshioka, J. Miyazaki, Physics of structural colors. *Rep. Prog. Phys.* **71**, 076401 (2008). doi:10.1088/0034-4885/71/7/076401
23. N. S. Hart, T. D. Lamb, H. R. Patel, A. Chuah, R. C. Natoli, N. J. Hudson, S. C. Cutmore, W. I. L. Davies, S. P. Collin, D. M. Hunt, Visual Opsin Diversity in Sharks and Rays. *Mol. Biol. Evol.* **37**, 811–827 (2020). doi:10.1093/molbev/msz269
24. E. Garza-Gisholt, R. M. Kempster, N. S. Hart, S. P. Collin, Visual Specializations in Five Sympatric Species of Stingrays from the Family Dasyatidae. *Brain Behav. Evol.* **85**, 217–232 (2015). doi:10.1159/000381091
25. S. M. Theiss, T. J. Lisney, S. P. Collin, N. S. Hart, Colour vision and visual ecology of the blue-spotted maskray, Dasyatis kuhlii Müller & Henle, 1814. *J. Comp. Physiol. A Neuroethol. Sens. Neural Behav. Physiol.* **193**, 67–79 (2007). doi:10.1007/s00359-006-0171-0
26. N. J. Marshall, F. Cortesi, F. de Busserolles, U. E. Siebeck, K. L. Cheney, Colours and colour vision in reef fishes: Past, present and future research directions. *J. Fish Biol.* **95**, 5–38 (2019). doi:10.1111/jfb.13849

27. J. Marshall, Vision and lack of vision in the ocean. *Curr. Biol.* **27**, R494–R502 (2017). doi:10.1016/j.cub.2017.03.012
28. U. E. Siebeck, N. J. Marshall, Ocular media transmission of coral reef fish--can coral reef fish see ultraviolet light? *Vision Res.* **41**, 133–149 (2001). doi:10.1016/s0042-6989(00)00240-6
29. G. S. Losey, T. W. Cronin, T. H. Goldsmith, D. Hyde, N. J. Marshall, W. N. McFarland, The UV visual world of fishes: a review. *J. Fish Biol.* **54**, 921–943 (1999). doi:10.1111/j.1095-8649.1999.tb00848.x
30. R. Chadyšiene, A. Girgždys, Ultraviolet radiation albedo of natural surfaces. *J. Environ. Eng. Landsc. Manage.* **16**, 83–88 (2008).doi:10.3846/1648-6897.2008.16.83-88
31. I. C. Cuthill, J. C. Partridge, A. T. D. Bennett, S. C. Church, N. S. Hart, S. Hunt, "Ultraviolet Vision in Birds" in *Advances in the Study of Behavior*, P. J. B. Slater, J. S. Rosenblatt, C. T. Snowdon, T. J. Roper, Eds. (Academic Press, 2000), vol. 29, pp. 159–214. doi:10.1016/S0065-3454(08)60105-9
32. M. D. Shawkey, G. E. Hill, Significance of a basal melanin layer to production of non-iridescent structural plumage color: evidence from an amelanotic Steller's jay (Cyanocitta stelleri). *J. Exp. Biol.* **209**, 1245–1250 (2006). doi: 10.1242/jeb.02115.
33. J. D. Forster, H. Noh, S. F. Liew, V. Saranathan, C. F. Schreck, L. Yang, J.-G. Park, R. O. Prum, S. G. J. Mochrie, C. S. O'Hern, H. Cao, E. R. Dufresne, Biomimetic isotropic nanostructures for structural coloration. *Adv. Mater.* **22**, 2939–2944 (2010). doi:10.1002/adma.200903693
34. M. D. Shawkey, L. D'Alba, J. Wozny, C. Eliason, J. A. H. Koop, L. Jia, Structural color change following hydration and dehydration of iridescent mourning dove (Zenaida macroura) feathers. *Zoology* . **114**, 59–68 (2011). doi:10.1016/j.zool.2010.11.001
35. D. Ge, L. Yang, G. Wu, S. Yang, Angle-independent colours from spray coated quasi-amorphous arrays of nanoparticles: combination of constructive interference and Rayleigh scattering. *J. Mater. Chem.* **2**, 4395–4400 (2014). doi:10.1039/C4TC00063C
36. M. M. Giusti, R. E. Wrolstad, Characterization and measurement of anthocyanins by UV-visible spectroscopy. *Curr. Protoc. Food Anal. Chem.* **00**, F1.2.1–F1.2.13 (2001). doi:10.1002/0471142913.faf0102s00
37. H. G. Frohnhöfer, J. Krauss, H.-M. Maischein, C. Nüsslein-Volhard, Iridophores and their interactions with other chromatophores are required for stripe formation in zebrafish. *Development*. **140**, 2997–3007 (2013). doi:10.1242/dev.096719
38. L. D. Faílde, R. Bermúdez, F. Vigliano, G. A. Coscelli, M. I. Quiroga, Morphological, immunohistochemical and ultrastructural characterization of the skin of turbot (Psetta maxima L.). *Tissue Cell*. **46**, 334–342 (2014). doi:10.1016/j.tice.2014.06.004
39. J. Oeffner, G. V. Lauder, The hydrodynamic function of shark skin and two biomimetic applications. *J. Exp. Biol.* **215**, 785–795 (2012). doi:10.1242/jeb.063040

40. M. V. Ankhelyi, D. K. Wainwright, G. V. Lauder, Diversity of dermal denticle structure in sharks: Skin surface roughness and three-dimensional morphology. *J. Morphol.* **279**, 1132–1154 (2018). doi:10.1002/jmor.20836
41. M. E. Rawles, Origin of melanophores and their role in development of color patterns in vertebrates. *Physiol. Rev.* **28**, 383–408 (1948). doi:10.1152/physrev.1948.28.4.383
42. J. D. Taylor, J. T. Bagnara, Dermal Chromatophoies. *Am. Zool.* **12**, 43–62 (1972). doi:10.1093/icb/12.1.43
43. Š. Moudříková, L. Nedbal, A. Solovchenko, P. Mojzeš, Raman microscopy shows that nitrogen-rich cellular inclusions in microalgae are microcrystalline guanine. *Algal Research*. **23**, 216–222 (2017). doi:10.1016/j.algal.2017.02.009
44. A. Jantschke, I. Pinkas, A. Hirsch, N. Elad, A. Schertel, L. Addadi, S. Weiner, Anhydrous β-guanine crystals in a marine dinoflagellate: Structure and suggested function. *J. Struct. Biol.* **207**, 12–20 (2019). doi:10.1016/j.jsb.2019.04.009
45. D. L. Fox, Animal biochromes and structural colours. 1976 Berkeley. *CA: University of California Press*.
46. Y. Kamishima, Electron Microscopic Study on Reflecting Platelets in the Dorsal Iridophores of the Sand Eel, Ammodytes personatus Girard. *Proc. Jpn. Acad. Ser. B Phys. Biol. Sci.* **54**, 634–639 (1978). doi:10.2183/pjab.54.634
47. D. Gur, Y. Politi, B. Sivan, P. Fratzl, S. Weiner, L. Addadi, Guanine-based photonic crystals in fish scales form from an amorphous precursor. *Angew. Chem. Int. Ed Engl.* **52**, 388–391 (2013). doi:10.1002/anie.201205336
48. A. Wagner, V. Ezersky, R. Maria, A. Upcher, T. Lemcoff, E. D. Aflalo, Y. Lubin, B. A. Palmer, The Non-Classical Crystallization Mechanism of a Composite Biogenic Guanine Crystal. *Adv. Mater.* **34**, e2202242 (2022). doi:10.1002/adma.202202242
49. Z. Eyal, R. Deis, N. Varsano, N. Dezorella, K. Rechav, L. Houben, D. Gur, Plate-like Guanine Biocrystals Form via Templated Nucleation of Crystal Leaflets on Preassembled Scaffolds. *J. Am. Chem. Soc.* **144**, 22440–22445 (2022). doi:10.1021/jacs.2c11136
50. E. J. Denton, Review lecture: on the organization of reflecting surfaces in some marine animals. *Philos. Trans. R. Soc. Lond. B Biol. Sci.* **258**, 285–313 (1970). doi:10.1098/rstb.1970.0037
51. A. Levy-Lior, E. Shimoni, O. Schwartz, E. Gavish-Regev, D. Oron, G. Oxford, S. Weiner, L. Addadi, Guanine-based biogenic photonic-crystal arrays in fish and spiders. *Adv. Funct. Mater.* **20**, 320–329 (2010). doi:10.1002/adfm.200901437
52. S. J. Dearden, A. Ghoshal, D. G. DeMartini, D. E. Morse, Sparkling Reflective Stacks of Purine Crystals in the Nudibranch Flabellina iodinea. *Biol. Bull.* **234**, 116–129 (2018). doi:10.1086/698012
53. R. O. Prum, R. L. Morrison, G. R. Ten Eyck, Structural color production by constructive reflection from ordered collagen arrays in a bird (Philepitta castanea: Eurylaimidae). *J. Morphol.* **222**, 61–72 (1994). doi:10.1002/jmor.1052220107

54. R. O. Prum, R. Torres, S. Williamson, J. Dyck, Two-dimensional Fourier analysis of the spongy medullary keratin of structurally coloured feather barbs. *Proceedings of the Royal Society of London. Series B: Biological Sciences*. **266**, 13–22 (1999). doi:10.1098/rspb.1999.0598
55. R. O. Prum, R. Torres, Structural colouration of avian skin: convergent evolution of coherently scattering dermal collagen arrays. *J. Exp. Biol.* **206**, 2409–2429 (2003). doi:10.1242/jeb.00431
56. R. O. Prum, J. A. Cole, R. H. Torres, Blue integumentary structural colours in dragonflies (Odonata) are not produced by incoherent Tyndall scattering. *J. Exp. Biol.* **207**, 3999–4009 (2004). doi:10.1242/jeb.01240
57. L. Schertel, L. Siedentop, J. Meijer, P. Keim, C. M. Aegerter, G. J. Aubry, G. Maret, The Structural Colors of Photonic Glasses. *Advanced Optical Materials*. **7** (2019), p. 1900442. doi: 10.1002/adom.201900442
58. G. Jacucci, S. Vignolini, L. Schertel, The limitations of extending nature's color palette in correlated, disordered systems. *Proc. Natl. Acad. Sci. U. S. A.* **117**, 23345–23349 (2020). doi:10.1073/pnas.2010486117
59. C. W. Mason, Structural Colors in Insects. I. *J. Phys. Chem.* **30**, 383–395 (1926). doi:10.1021/j150261a009
60. E. Finger, Visible and UV coloration in birds: Mie scattering as the basis of color in many bird feathers. *Naturwissenschaften*. **82** (1995), pp. 570–573. doi: 10.1007/bf01140249
61. R. O. Prum, R. H. Torres, S. Williamson, J. Dyck, Coherent light scattering by blue feather barbs. *Nature*. **396** (1998), pp. 28–29. doi: 10.1038/23838
62. R. O. Prum, R. Torres, C. Kovach, S. Williamson, S. M. Goodman, Coherent light scattering by nanostructured collagen arrays in the caruncles of the malagasy asities (Eurylaimidae: aves). *J. Exp. Biol.* **202 Pt 24**, 3507–3522 (1999). doi:10.1242/jeb.202.24.3507
63. R. O. Prum, R. H. Torres, A fourier tool for the analysis of coherent light scattering by bio-optical nanostructures. *Integr. Comp. Biol.* **43**, 591–602 (2003). doi:10.1093/icb/43.4.591
64. J. Ballato, J. Dimaio, A. James, E. Gulliver, Photonic band engineering through tailored microstructural order. *Appl. Phys. Lett.* **75**, 1497–1499 (1999). doi:10.1063/1.124734
65. L. F. Rojas-Ochoa, J. M. Mendez-Alcaraz, J. J. Sáenz, P. Schurtenberger, F. Scheffold, Photonic properties of strongly correlated colloidal liquids. *Phys. Rev. Lett.* **93**, 073903 (2004). doi:10.1103/PhysRevLett.93.073903
66. P. D. García, R. Sapienza, Á. Blanco, C. López, Photonic glass: A novel random material for light. *Adv. Mater.* **19**, 2597–2602 (2007). doi:10.1002/adma.200602426
67. S. Magkiriadou, J.-G. Park, Y.-S. Kim, V. N. Manoharan, Absence of red structural color in photonic glasses, bird feathers, and certain beetles. *Phys. Rev. E Stat. Nonlin. Soft Matter Phys.* **90**, 062302 (2014). doi:10.1103/PhysRevE.90.062302

68. S. Magkiriadou, J.-G. Park, Y.-S. Kim, V. N. Manoharan, Disordered packings of core-shell particles with angle-independent structural colors. *Opt. Mater. Express*. **2**, 1343 (2012). doi:10.1364/ome.2.001343
69. J.-G. Park, S.-H. Kim, S. Magkiriadou, T. M. Choi, Y.-S. Kim, V. N. Manoharan, Full-spectrum photonic pigments with non-iridescent structural colors through colloidal assembly. *Angew. Chem. Int. Ed Engl.* **53**, 2899–2903 (2014). doi:10.1002/anie.201309306
70. R. O. Prum, R. H. Torres, Structural colouration of mammalian skin: convergent evolution of coherently scattering dermal collagen arrays. *J. Exp. Biol.* **207**, 2157–2172 (2004). doi:10.1242/jeb.00989
71. G. Shang, M. Eich, A. Petrov, Photonic glass based structural color. *APL Photonics*. **5**, 060901 (2020). doi:10.1063/5.0006203
72. Y. Takeoka, Angle-independent structural coloured amorphous arrays. *J. Mater. Chem.* **22**, 23299–23309 (2012). doi:10.1039/C2JM33643J
73. A. L. Davis, K. N. Thomas, F. E. Goetz, B. H. Robison, S. Johnsen, K. J. Osborn, Ultra-black Camouflage in Deep-Sea Fishes. *Curr. Biol.* **30**, 3470–3476.e3 (2020). doi:10.1016/j.cub.2020.06.044
74. S. Kawaguti, Y. Kamishima, Electron microscopic study on the iridophores of opisthobranchiate mollusks. *Biol. J. Okayama Univ* (1964).
75. N. Pinsk, A. Wagner, L. Cohen, C. J. H. Smalley, C. E. Hughes, G. Zhang, M. J. Pavan, N. Casati, A. Jantschke, G. Goobes, K. D. M. Harris, B. A. Palmer, Biogenic Guanine Crystals Are Solid Solutions of Guanine and Other Purine Metabolites. *J. Am. Chem. Soc.* **144**, 5180–5189 (2022). doi:10.1021/jacs.2c00724
76. M. Iwasaka, H. Asada, Floating photonic crystals utilizing magnetically aligned biogenic guanine platelets. *Sci. Rep.* **8**, 16940 (2018). doi:10.1038/s41598-018-34866-x
77. F. H. Mollen, Making Louis Agassiz's wish come true: combining forces and a new protocol for collecting comparative skeletal material of sharks, skates and rays, as a comment and an addition to "The need of providing tooth morphology in descriptions of extant elasmobranch species" by Guinot et al.(2018). *Zootaxa*. **4571**, 295–300 (2019).

Supplementary Files

This is a list of supplementary files associated with this preprint. Click to download.

- SurapanenietalSI.pdf